Title
Nano-imaging enabled via self-assembly

Journal
Nano Today, 9(5)

ISSN
1748-0132

Authors
McLeod, Euan
Ozcan, Aydogan

Publication Date
2014-10-01

DOI
10.1016/j.nantod.2014.08.005

Peer reviewed

Published in final edited form as:
Nano Today. 2014 October 1; 9(5): 560–573. doi:10.1016/j.nantod.2014.08.005.

Nano-imaging enabled via self-assembly

Euan McLeod and **Aydogan Ozcan**

SUMMARY

Imaging object details with length scales below approximately 200 nm has been historically difficult for conventional microscope objective lenses because of their inability to resolve features smaller than one-half the optical wavelength. Here we review some of the recent approaches to surpass this limit by harnessing self-assembly as a fabrication mechanism. Self-assembly can be used to form individual nano- and micro-lenses, as well as to form extended arrays of such lenses. These lenses have been shown to enable imaging with resolutions as small as 50 nm half-pitch using visible light, which is well below the Abbe diffraction limit. Furthermore, self-assembled nano-lenses can be used to boost contrast and signal levels from small nano-particles, enabling them to be detected relative to background noise. Finally, alternative nano-imaging applications of self-assembly are discussed, including three-dimensional imaging, enhanced coupling from light-emitting diodes, and the fabrication of contrast agents such as quantum dots and nanoparticles.

Keywords

Nano-imaging; self-assembly; nano-lenses; super-resolution; micro-lenses

1. INTRODUCTION

Nano-imaging, the process of imaging object features at length scales below ~200 nm, or approximately one-half the wavelength of visible light, is a burgeoning field with many applications in biomedical imaging [1–3], electronics and materials inspection [4,5], and fundamental physics such as plasmonics [6]. Progress in nano-imaging generally attempts to either improve sensitivity to particularly small objects, or to improve resolution in order to discriminate two closely-spaced small objects. Implementations of nano-imaging often require structuring devices at the nanometer length scale.

Self-assembly is the process of individual dispersed components naturally adopting desired configurations without being directly positioned. It is a popular area of current research for its potential in fabricating large numbers of structures in parallel, and in fabricating nano-scale structures in particular [7]. Self-assembly has been used to synthesize structures out of individual atoms [8], molecules [9,10], and larger components such as spherical microbeads [11]. Generally, the term self-assembly is only used when specialized structures with

nanoscale or microscale dimensions are formed. In contrast, the simple crystallization of a solid material from molten form would typically not be called self-assembly.

Despite the significant overlap in the size scales involved in nano-imaging and self-assembly, it is only recently that the two fields have converged. In this review, we highlight the nature of this convergence. To place these developments in context, we begin with a quick overview of the most popular existing nano-imaging systems, followed by a quick review of the most popular self-assembly techniques. We then discuss in more depth the synergy between nano-imaging and self-assembly, focusing on the use of self-assembly to fabricate micro- and nano-lenses and other imaging tools. We also briefly discuss the use of self-assembly in fabricating nano-scale contrast agents such as nanoparticles and quantum dots for use in conventional fluorescence microscopy, and in the use of self-assembled nano-scale features in coupling LED emission to the far-field, which is not an imaging problem per-se, although it shares much of the same physics.

1.1 Nano-imaging

Due to diffraction of light, conventional microscopy has a “practical” resolution limit of $\sim\lambda/(2NA)$, called the Abbe diffraction limit, where λ is the free-space optical wavelength and *NA* is the numerical aperture of the microscopic imaging system. When operating in air, $NA \leq 1$, and therefore for the shortest visible light (i.e., $\lambda = 400$ nm), the corresponding diffraction limit is approximately $\lambda/2 = 200$ nm. For small isolated structures, an added challenge in optical microscopy is capturing a strong enough signal to detect them relative to the background noise found in any imaging system. Depending on the nano-imaging application, sensitivity to isolated nanoscale features may be sufficient, and nano-scale resolution may not be needed.

The diffraction limit also applies to optical lithography. In lithography, the problem is however reversed in that diffraction limits into how small of an area light can be focused, as opposed to the ability to generate a sharp magnified image, as is the case in microscopy. Despite this difference, there is much overlap between the two fields, and strategies (such as self-assembly) that work well for nano-lithography can often also be successfully applied to nano-imaging, as will be detailed below.

One of the oldest ways of improving resolution beyond 200 nm is to increase the lens *NA* beyond 1.0 using an immersion medium between the object and the objective lens, as *NA* is proportional to the refractive index of the immersion medium. Most commonly, the immersion medium is an oil with refractive index equal to that of glass, or about 1.5. However other types of immersion liquids may be used [12], as well as solid materials, which are called solid immersion lenses (SILs) [4,13,14]. These SILs, if they are of wavelength size scale or smaller, can also improve resolution through additional shape-dependent and size-dependent nanophotonic mechanisms, as discussed in greater detail below.

Another early method of nano-imaging is the near-field scanning optical microscope (NSOM or SNOM) [15–18]. This device is practically similar to an atomic force microscope (AFM) in that a sharp probe tip is mechanically scanned across a surface while maintaining

contact (or a very small gap of < 100 nm) with the surface. In contrast to an AFM, however, the NSOM is used to concentrate or collect/probe light via its sharp tip. Several different schemes have been used to do this, many of which involve a hollow tip with a small aperture at the apex with diameter below the diffraction limit. Because the tip is maintained close to the object, the exponential decay of higher spatial frequencies that make up the object's spatial spectrum is significantly mitigated compared to far-field optical microscopy. Unlike lens-based traditional microscopy, the resolution limit in NSOM is mostly determined by (i) the tip aperture size plus twice the skin-depth of the optical field inside the NSOM tip material (e.g., aluminum), and (ii) the 3D precision with which the tip can be positioned and scanned relative to the object topology. With tip apertures of 50 nm and smaller, NSOM can achieve a high spatial resolution (typically ~50–500 nm), although often at great inconvenience due to the tradeoffs of very low transmittance through such small apertures, slow image acquisition time as a result of scanning, complications in 3D alignment, and the need for physical access within ~100 nm of the object features. The same conclusions, by and large, hold for all three modes of operation for NSOM systems, i.e., illumination, collection and scattering (or apertureless).

In the past decade, a host of methods have been developed to provide sub-diffraction limit resolution that can potentially resolve some of the problems associated with NSOMs. One approach that can provide an improvement in diffraction-limited resolution is a synthetic aperture approach, which is typically combined with interferometric microscopy or digital holography [19–23]. In conventional microscopy, the resolution is determined by the numerical aperture, which is proportional to the physical aperture size at the exit pupil plane of an imaging system. This aperture function, acting like a low-pass spatial filter, rejects the high spatial frequency information that is carried by travelling waves, corresponding to some of the unresolved details of an image. In the synthetic aperture method, a grazing-incidence (or evanescent in some cases [19]) off-axis light illumination may be used to shift the high-spatial frequency content of the specimen into the pass-band of the imaging system [20], or an additional element may be inserted in the optical train that scatters high spatial frequencies and redirects them back inside the physical aperture of the pupil function [21–23]. In the latter case, the recorded image is no longer a true image of the object due to frequency mixing, however the true image can be computationally synthesized using the recorded image.

Another super-resolution approach is to develop metamaterial hyperlenses and super-lenses [24–27]. This approach involves making a lens out of a man-made material that is structured at sub-wavelength scales, typically with alternating layers of metals and dielectrics. When designed appropriately, these materials can have a negative index of refraction, which inverts the effects of diffraction, amplifying the higher spatial frequencies that would normally follow an exponential decay in free space. Such lenses still require placement in the near-field of the object similar to an NSOM, however depending on the design, they may not require scanning to form an image. On the other hand, a scanning-free operation also means it is very challenging to have a space-invariant transfer function since such metamaterial based lenses would have difficulty to exactly follow the 3D topology of an "arbitrary" object, limiting their potential use to 2D (i.e., flat) objects. Another limitation of

such an approach is the aberrations created by fabrication imperfections as well as undesired modulation and degradation of lower spatial frequencies of the object.

A highly successful fluorescent nano-imaging technique is stimulated emission-depletion (STED) microscopy [3,28]. Here, a high-intensity laser beam is used to temporarily bleach a doughnut-shaped region of the fluorescent sample of interest. A second, lower-power laser beam is used in parallel to the first beam to fluorescently excite the same spot of the object. Although both laser beams are diffraction-limited, the resulting image has resolution beyond the diffraction limit because the power of the first beam can be controlled in a nonlinear fashion so as to only leave an arbitrarily-small region at the center of the doughnut unbleached, i.e., fluorescent. In other words, although the full-width at half-minimum of the doughnut is of order $\lambda/(2NA)$, the full-width at bleaching threshold can be significantly smaller. Both laser beams are then scanned together across the whole sample to form a full fluorescent image of the object.

Other fluorescent nano-imaging approaches also depend on fluorophores that can be turned on and off (e.g., by bleaching). Such techniques are in general referred to as photoactivatable or photoswitchable fluorescent microscopy [2]. Two particularly prominent examples are photoactivated localization microscopy (PALM) [29] and stochastic optical reconstruction microscopy (STORM) [30]. In these methods, fluorophores are initially prepared in a dark (i.e. non-fluorescent) state, and then a random fraction of these fluorophores are converted to a bright (fluorescent) state for a short period of time by laser irradiation. If only one fluorophore in a small region is activated at any given time, then its location can be determined with nanometer-level precision by calculating the centroid of its point spread function. Through multiple cycles of this procedure, a complete mapping of all of the individual fluorophores can be performed dot-by-dot, thereby generating a full-field high-resolution image. The success of these techniques is critically dependent on the type of fluorophore used; it must have the capability to be optically activated, excited, and subsequently deactivated, or bleached. Depending on the type of fluorophore, these three steps may all be driven by the same light source, or may be controlled via separate sources. In recent years, various new fluorophores have been developed, including those based off of standard laser dyes, as well as genetically-encodable fluorophores such as green fluorescent protein (GFP).

1.2 Self-assembly

Self-assembly approaches rely on random motion of the individual components in order for each component to explore its energy potential landscape and find a thermodynamically (meta-) stable configuration. Most often, this random motion is driven by Brownian motion, the random thermal fluctuations in liquid environments. For such fluctuations to be significant, individual components need to have length scales below ~10 μm. There is no practical lower limit on the size scale of the individual components, and indeed, self-assembly has been used to form desired structures out of individual atoms and molecules [8,10]. In addition to Brownian motion, other types of random motion may be used to allow components to find optimal configurations, such as convection [31] or vibration [32]. These other forces can enable the self-assembly of even larger scale objects [7]. Sometimes it is the

interplay between these random forces and a body force (e.g., gravity or applied electric fields) that leads to the self-assembly of regular structures [11,33]. Many different self-assembly approaches exist. Below, we introduce a few of the most common examples.

Volmer-Weber and Stranski-Krastanov growth, the methods by which quantum dots may be grown on smooth, flat substrates is a form of self-assembly [34]. Here, individual atoms from the vapor phase adsorb on a surface. Due to surface energy effects, these atoms may tend to cluster in isolated islands (or layers and then islands), which can become InAs/GaAs quantum dots, for example [35].

Biologically-inspired self-assembly methods are also used. One of the most popular is to use complimentary DNA strands to bind objects together. In this process, aptamers (short segments of DNA) with a specific sequence are bound to one component. Aptamers with the complementary sequence are then bound to the other component. Upon mixing, the two components will spontaneously bind together through the DNA-DNA interaction [36]. This principle has been used to fabricate rather complex structures from a smaller library of simple building blocks [37]. DNA-DNA interaction can also be used to self-assemble larger, micro-scale structures, for example out of hydrogel building-blocks [38]. Hydrogels and their assembly into complex structures are particularly useful for tissue engineering applications because of their biocompatibility and potential for housing embedded cells [39]. Antibody-antigen interactions can also be used in a similar way as DNA-DNA interactions to self-assemble structures [40].

Self-assembly has been frequently used to create a highly uniform single layer of molecules on a surface, called a self-assembled-monolayer. Typically, the molecules used are carbon chains with a functional group at the free surface and either a thiol group (for adsorption to gold) or a silane group (for covalent bonding to oxide) at the substrate [41].

Diblock-copolymers form another frequently-used medium for self-assembly [9]. Diblock copolymers are two different types of polymer chains that are covalently linked end-to-end. Due to the difference in intermolecular interaction energy between the two different types of polymers, they tend to self-assemble into nanoscopic domains that are primarily composed of only one type of polymer. However, the fact that the two types of polymers are covalently bound to each other prevents macroscopic phase separation and limits the length scale of these domains. Depending on the types and relative lengths of the chains, a number of different microscopic phases are possible.

Surface tension can also be a useful driving force for the self-assembly of structures [42]. When a liquid spans two solid objects, the force of surface tension can be used to pull the two objects together. If the objects' shapes are designed intelligently, and the liquid is located at the correct place, complex assemblies can be formed, even of large-scale objects. At smaller length scales, surface-tension is important for ensuring smooth surfaces on self-assembled structures. Smoothness is an important optical consideration because smooth surfaces tend to be low-loss and exhibit reduced scattering, which are very important for e.g., waveguides, optical cavities, or resonators. Improving the smoothness in pre-fabricated structures is possible by thermal reflow, where the structure is heated just barely above the

melting point (or glass transition temperature, depending on the material), enough so that rough areas will smoothen due to surface tension, but the structure itself will not completely flow away.

In the self-assembly of arrays of spherical particles, the most common approach is via evaporation of the solvent from a suspension of micro- or nano-spheres [43,44]. Due to surface tension, spheres naturally self-assemble into hexagonally-close-packed arrays at the boundary of the evaporation front. Other more complicated methods also exist for forming self-assembled arrays of microspheres, such as self-assembly during spin-coating, self-assembly at air-liquid interfaces, and self-assembly in electric fields [11].

The self-assembly of arrays of spheres is particularly relevant in this review because of their use as imaging lenses. Individual micro-lenses and micro-lens arrays have numerous applications, including sensitivity enhancement for CMOS and CCD image sensors [45], imaging of light-fields in Shack-Hartmann sensors [46] and computational photography [47–49], as well as surface patterning and lithography [11]. Micro-lenses have also been naturally self-assembled in biological organisms such as insects [50] and brittlestars [51]. In one example, bordering on nano-imaging, Huang, Lu, and Yeh used dielectrophoresis and a templated substrate to produce a particularly low-defect array of particles in non-close-packed geometries. Although their results did not provide sub-diffraction-limit imaging, they nonetheless demonstrated a relatively good resolution of ~400 nm, corresponding to an effective NA of 0.8 [52].

2. APPLICATIONS OF SELF-ASSEMBLY TO NANO-IMAGING

2.1 Signal enhancement in nano-imaging via self-assembled micro and nano-lenses

One application of micro/nano lenses in nano-imaging is to aid in the detection of nanoscale objects, either via scattering or fluorescence. For these applications, the critical factor is typically not resolution, but instead signal enhancement or signal-to-noise ratio (SNR). While manual positioning methods have been used to position or scan lenses across a substrate [13,14], self-assembly can greatly simplify the alignment between the lens and the nanoscale object of interest.

An early example of this concept was demonstrated by Brody and Quake where they used self-assembly via a biotin-streptavidin interaction to attach a 200 nm fluorescent particle to a 1.1 μm microsphere, which acted as a lens (Figure 1) [53]. This two-particle assembly was then used to measure rotational diffusion rates in liquid solutions by observing the blinking signal caused by enhanced fluorescence when the larger sphere happened to be correctly aligned to direct the fluorescent emission toward the microscope objective. This provided intensity enhancements of approximately 9-fold when using a 0.4 NA objective. This same concept has more recently been applied to the detection of single molecules, where the 200 nm fluorescent bead has been substituted with a single, fluorescently-labeled molecule tethered to a substrate (Figure 2) [54]. Here, the use of the large microsphere provided several benefits, including the ability to enhance the photostability of the fluorophore, and the ability to use lower numerical aperture lenses (20X, 0.5 NA) which increased the field of view and working distance. The long working distance allowed the substrate to be

maintained at a different temperature relative to the objective. Without the colloidal micro-lenses, a 1.43 NA objective was required to obtain comparable signal levels.

Achieving the strong signal levels necessary to see small particles has also been a recent focus in holographic on-chip microscopy. Holographic microscopy records the interference between a reference wave of light and the wave scattered from the object under investigation. Of particular recent interest is lensfree holographic computational microscopy, where no imaging lenses are necessary [55–59]. In this method, interferograms are recorded directly on a CCD or CMOS imaging chip, and images of the original objects are reconstructed computationally. When the object is particularly small, the amplitude of the scattered wave is much weaker than that of the reference wave, and the resulting interference signal may be lost within the background noise. Two new approaches to solve this problem have been to form either self-assembled liquid catenoid-shaped nano-lenses (Figure 3) [60,61] or a continuous liquid wetting film [55,62,63] around the target particles on a chip. These two approaches serve similar purposes in that they greatly increase the scattering cross section of the nanoparticles, and thereby improve the threshold for detection in these holographic systems from approximately 300 nm to below 100 nm. This has enabled lensfree holographic microscopy techniques to reach the domain of imaging single viruses across very large imaging fields-of-view, e.g., >20–30 mm^2 or >10 cm^2, using CMOS or CCD imaging chips, respectively [60,61].

2.2 Resolution enhancement in nano-imaging via self-assembled micro- and nano-lenses

Despite their conventional material composition and typical illumination schemes, dielectric lenses with wavelength-scale dimensions can also provide spatial resolution in the sub-200 nm regime [64–68]. Much of this effect is due simply to the higher refractive index of the lens medium (the immersion lens effect). However, some added bonus appears to occur due to the geometrical shape and wavelength-scale size of the lens. Most commonly, these effects are investigated by looking at the inverse problem: how small of a focal spot is possible when coupling far-field light into the micro- or nano-lens. This approach applies best to the case where these lenses are used for lithography [69–71], but it is naturally expected that measurements of focal spot size will correlate with imaging resolution. In one such study, Fletcher, Goodson, and Kino showed using Mie theory that wavelength-scale microspheres can generate focal spots as much as 25% smaller than that predicted by vector diffraction theory, which is valid for larger length scales [72]. Mason, Jouravlev, and Kim found a similar result, showing through finite-difference time-domain (FDTD) simulations, that the width of the focal spot behind a wavelength-scale solid immersion lens can be as much as 25% smaller than that generated by a macroscopic SIL of equal refractive index [64,73]. Using both ray tracing and FDTD simulations, Guo et al. investigated what size and refractive index of microspheres generated the smallest spot sizes behind the microspheres [67]. They found that the optimal refractive index contrast between the sphere and medium lay between 1.5 and 1.75, while the optimal sphere radii lay between 1.125 λ/n_0 and 1.275 λ/n_0, where n_0 is the background medium refractive index. The smallest focal spot width they could obtain using 400 nm light was 104 nm FWHM using a 900 nm diameter sphere and a refractive index contrast of 1.75.

Studies that investigate the use of micro and nano-lenses specifically as imaging devices are rarer. Based on Mie theory, Duan, Barbastathis, and Zhang concluded that the best resolution such spherical lenses could theoretically achieve was between 100 and 150 nm – somewhat smaller than the Abbe limit [74]. They also acknowledge that other effects not included in the Mie theory (e.g., surface roughness, plasmonics, different geometrical lens shapes) could further enhance resolution.

With strong theoretical evidence of the potential for sub-diffraction-limit imaging using dielectric micro-lenses, the challenge becomes fabrication of the optimal lens geometry. Self-assembly has proven to be an attractive way to fabricate these individual dielectric nano-lenses. Lee et al. self-assembled spherical cap-shaped nano-lenses out of calix [4] hydroquinone (CHQ) (Figure 4). This molecule can be used to construct a variety of nanostructures, including nanotubes, nanospheres, and plano-convex structures, which have displayed the most promise as nano-lenses [73,75]. They used these lenses to resolve lines with a pitch (period) as small as 220–250 nm in conjunction with a 0.9 NA 100X objective lens. The Rayleigh resolution limit for the same objective lens without nano-lenses is $0.61\frac{\lambda}{NA}=320\,\mathrm{nm}$. Here, these nano-lenses provide enhanced resolution through a combination of the solid immersion lens effect (CHQ has a refractive index of 1.5), and the nano-lensing effect due to the wavelength-scale size of the lens.

In addition to molecular self-assembly from molecules dissolved in a solvent, surface tension at an air-liquid interface can also be used to drive self-assembly. This technique has been used successfully by many groups to form extended and highly regular micro-lens arrays, typically by fabricating a regular array of polymer pillars using photolithography, and then heating this array above the melting temperature to allow thermal reflow [65,66,76]. Thermal reflow can also be used on adsorbed colloidal spheres to fabricate plano-convex lenses [52,77]. Depending on the temperature and annealing time, surfaces with nonuniform curvature across the curved face are possible (Figure 5). In one study, such lenses performed better than either complete spheres or spherical caps, enabling spatial features as small as 170–180 nm to be resolved [77].

Perfectly spherical beads have also been successfully used as nanoimaging lenses. In contradiction to the previous results, Wang et al. found complete spheres to perform better than the typical plano-convex SIL shape. They used 3 μm spheres assembled on a surface to image patterns on the substrate with a half-pitch as small as 50 nm (Figure 6) [68]. Here, evaporative self-assembly has been harnessed to enable closely-packed monolayers of microspheres. As this is one of the best experimental resolutions demonstrated to-date, it is apparent that perfectly spherical lenses perform well as high-resolution nano-imagers.

The use of surface tension to drive self-assembly has recently been extended to the realm of nano-scale lenses using dip-pen nanolithography [71]. In dip-pen nanolithography [78], a sharp tip similar to an AFM cantilever is dipped in a liquid material, and then lightly touched to a target substrate. When performed correctly, a small amount of material is transferred from the tip onto the substrate. Jang et al. used this technique to form arrays of 900 nm nano-lenses out of poly ethylene glycol (PEG) which were subsequently used for

focusing in near-field nanolithography to form features with length scales of approximately 100 nm. Although used only for lithography here, such lenses could also be used for imaging applications in the future in a scheme similar to that presented in [75]. It is also possible to fabricate liquid nano-lenses at room temperature using methods such as dip-pen nanolithography and then subsequently photopolymerize them to form permanent solid lens structures [79,80].

Similar to dip-pen nanolithography, a PDMS stamp with lithographically-defined nanopillars can also be used to transfer liquid nano-lenses from a liquid reservoir to a substrate (Figure 7). Kang et al. used this method to form spherical-cap liquid nano-lenses with diameters ranging from 481 nm to 15.5 μm and contact angles ranging from 9.8° to 90.9° [81]. These lenses could be made from UV-curable polymer to ensure long-term stability. Using 3 μm diameter lenses with 90.9° contact angle, in conjunction with a 150X 0.9 NA microscope objective, they were able to resolve nanoscale gaps as small as 130 nm.

Liquid droplets have also been used as lenses for light propagating parallel to a substrate instead of perpendicularly to it. Smolyaninova et al., used droplets of glycerin on a substrate as nano-magnifiers in this fashion [82,83]. For metal substrates, they invoke plasmonics and surface plasmon polariton physics to explain the observed imaging behavior and their ability to achieve resolution on the order of $\lambda/8$ [83]. However, they also observe similar results on non-plasmonic substrates, where they argue that these lenses perform analogously to the metamaterial fish-eye and Eaton lenses, without the need for metallic components [84]. They showed that theses lenses on non-plasmonic substrates were capable of imaging and magnifying light from an NSOM probe tip, however they did not quantify the resolution.

Another approach to the self-assembly of liquid nano-lenses is to harness dewetting to transform an originally continuous film into an array of individual nano-lens droplets. In this process, a thin polymer film is spun-coat from a binary solution of polymer molecules and solvent. As the solvent evaporates, a solid continuous polymer film is left behind. When this film is heated above the polymer glass transition temperature, the film may spontaneously break up into individual droplets, driven by either van der Waals interactions [85–87] or temperature gradients [88,89]. The nature of the break-up and morphology of the droplets depends on the surface energy of the substrate and the original film thickness (Figure 8). If some sort of lithographic patterning is used to provide a periodic initial configuration of the film, then a highly regular array of droplets may be formed. Verma and Sharma have used this procedure to produce ~90 nm and larger diameter nano-lenses [86,87]. In a later study, they used self-assembled dewetted lenses as immersion lenses to enable imaging of 500 nm wide stripes in conjunction with a 50X NA 0.5 microscope objective [85,87]. The Rayleigh resolution limit for such an objective is 0.61 λ/NA = 4.90 nm, which places their experimental results right at the resolution limit.

2.3 Other applications of self-assembly in nano-imaging and light-emission

Beyond 2D imaging, nano-lenses have also been used as integral imagers to capture 3D light-field information about microscopic objects [47]. Rajasekharan et al. used electronically-controlled liquid crystal arrays of lenses to capture 3D information of microscopic objects and then re-project magnified versions of this information using a 3D

display [90]. Although the lenses were particularly small (micron scale or smaller), spatial resolution was not quantified. The fabrication of this lens array is particularly interesting because regular arrays of bundles of carbon nanotubes were used as seeds to direct the formation of the liquid-crystal nano-lenses under an applied voltage [91]. In another use of liquid-crystals, self-assembled focal conic domains exhibit nano-lens-like properties over large arrays, however they have not yet been applied to any practical devices [92]. The ability to dynamically control the shape of liquid crystal structures is likely to enable advanced imaging and/or sensing applications.

The use of shape-memory materials also provides a unique approach to fabricating nano-lenses. Although Jeon et al. used conventional methods (photolithography and replication molding) to initially form a nano-lens array, they fabricated the array out of a shape-memory polymer [93]. After deformation and subsequent re-heating, the nano-lens array “self re-assembled” to its original state. This approach may be used to fabricate particularly robust nano-imaging devices in the future.

Self-assembled nanostructures with morphologies other than lens-shapes can also be used for nano-imaging. Khokhra et al. have shown that nano-sheets of ZnO self-assembled from a solution can be used to create a turbid lens with an effective NA of ~2.0 [94]. A turbid lens is a highly scattering but transmissive film. The scattering enables the collection of photons leaving the sample at high angles, although it also scrambles these photons so that a direct image of the object cannot be formed using conventional optics. However, by performing a detailed characterization of the scattering properties of the film, the nature of the scrambling can be deduced (or calibrated), and the scrambled image might be computationally descrambled [95,96]. Although Khokra et al. did not actually perform this unscrambling or resolve nano-scale objects, they demonstrated the effective increase in NA by angularly scanning a laser beam and measuring at what angles scattered light could be collected by the microscope objective. In this experiment, the initial microscope objective NA was ~0.9, which became approximately 2.0 with the addition of the turbid lens element.

In addition to their uses in imaging and lithography, the self-assembly of nano-lenses has been used to increase the emission efficiency of light-emitting diodes (LEDs). Zhang et al. used spin-coating to deposit a self-assembled monolayer of nanospheres on the surface of LEDs, which were subsequently used as lithographic masks for depositing ITO nano-lenses on top of the surface [97]. This improved the overall efficiency of the LEDs by up to 63.5%, and also improved the directionality of the emission. Ee et al. used self-assembly to deposit close-packed micron-scale diameter silica spheres, in some cases with an additional polymer layer to fill the interstitial regions up to the equator of the microspheres [98]. This provided light extraction efficiencies up to 2.6 times greater than without the lens arrays. Sun et al. grew self-assembled GaN nanolenes on blue InGaAs LEDs using a multi-step lithography and etching procedure using CsCl islands as a mask [99]. The surface of the LED in this experiment was also covered by nanocones in the interstitial regions between the hemispherical lenses. Of the sizes they tried, hemispherical lenses with 800 nm diameter performed best, with an enhancement in emissivity of 1.9-fold. Son, Jung, and Park performed a similar study, although they particularly investigated the difference between nanocone and nanohemisphere morphologies. They fabricated different types of ZnO

nanostructures on GaN green LEDs by self-assembly in aqueous solution [100]. They found that ~1 μm (but with much dispersion in size) hemispherical nano-lens-shaped ZnO structures enhanced emission by approximately 7-fold. Nanorod and nanocone ZnO structures did not provide as much of an enhancement.

2.4 Contrast agents

There are many studies involving the use of nanoparticles and assemblies of nanoparticles as contrast agents for biological imaging. As this work has already been covered extensively in various reviews, e.g. [1,101–104], we will only briefly mention here some of the ways self-assembly is used to form contrast agents without providing an exhaustive review of the studies involved.

Self-assembled colloidal quantum dots are often used as contrast agents in place of fluorophores in fluorescent microscopy. Quantum dots provide higher brightness and greater long-term stability, and better spectral characteristics than fluorescent molecules, however they can also exhibit blinking which can result in unstable image brightness [105,106]. Self-assembly plays an important role in the use of quantum dots because it provides a mechanism for their initial formation through the interaction of the individual atomic components and surfactants, as well as the potential later clustering of the quantum dots into larger assemblies [101].

Metallic nanoparticle agents form another contrast option. Here, the plasmon resonance of these particles endows them with unique optical properties that can be identified when using a broadband, or frequency-scanning source. When these particles cluster (possibly due to a self-assembly process), their plasmon resonance can shift, changing their apparent color (Figure 9) [107,108]. When the nanoparticles are biochemically labeled, clustering-induced color changes can be used to identify regions with high concentration of a specific biological or chemical marker/agent [101,107,109]. Self-assembled metallic nanoparticles can also be used in Raman imaging, which interrogates the vibrational modes of molecules [110].

3. CONCLUSION

Many approaches to imaging below the diffraction limit require the fabrication or positioning of structures at length scales below ~10 μm. Self-assembly has been found to be an excellent fabrication method for these applications, as it also typically functions at these length scales. The use of self-assembly techniques in nano-imaging applications has led to new avenues for nanoscopy, including signal enhancement for the detection of small objects, resolution enhancement through near-field focusing for half-pitch resolutions as small as 50 nm, 3D imaging capabilities, and emissivity enhancement. By and large, these approaches have relied on easily available common dielectric materials. It is likely that future studies building on these approaches will bring further enhancements including finer resolution, larger fields of view, and better control over the relative positioning between these self-assembled nano-imagers and their 3D nano-scale targets. One avenue of significant improvement in the near future is likely to come from the self-assembly of nano-imagers made out of multiple material components. The large majority of the nano-imagers presented here are fabricated out of a single functional material. Through the use of multiple

material components, more complicated optical systems that can provide precision photon guidance are possible, as well as the fabrication of intelligently-designed metamaterial devices. We expect these innovations to provide even finer resolutions and higher optical sensitivities.

Acknowledgments

Ozcan Research Group at UCLA gratefully acknowledges the support of the Presidential Early Career Award for Scientists and Engineers (PECASE), Army Research Office (ARO) Life Sciences Division, ARO Young Investigator Award, National Science Foundation (NSF) CAREER Award, NSF CBET Division Biophotonics Program, NSF Emerging Frontiers in Research and Innovation (EFRI) Award, Office of Naval Research (ONR), the Howard Hughes Medical Institute (HHMI), and National Institutes of Health (NIH) Director's New Innovator Award DP2OD006427 from the Office of the Director, National Institutes of Health. This work is based upon research performed in a renovated laboratory by the National Science Foundation under Grant No. 0963183, which is an award funded under the American Recovery and Reinvestment Act of 2009 (ARRA).

References

1. Koo H, Huh MS, Ryu JH, Lee DE, Sun IC, Choi K, Kim K, Kwon IC. Nano Today. 2011; 6:204.
2. Heilemann M. J Biotechnol. 2010; 149:243. [PubMed: 20347891]
3. Hell SW. Science. 2007; 316:1153. [PubMed: 17525330]
4. Ippolito SB, Goldberg BB, Ünlü MS. Appl Phys Lett. 2001; 78:4071.
5. Holler M, Raabe J, Diaz A, Guizar-Sicairos M, Quitmann C, Menzel A, Bunk O. Rev Sci Instrum. 2012; 83:073703. [PubMed: 22852697]
6. Kawata S, Inouye Y, Verma P. Nat Photonics. 2009; 3:388.
7. Whitesides GM, Grzybowski B. Science. 2002; 295:2418. [PubMed: 11923529]
8. Leonard D, Pond K, Petroff PM. Phys Rev B. 1994; 50:11687.
9. Park M, Harrison C, Chaikin PM, Register RA, Adamson DH. Science. 1997; 276:1401.
10. Schreiber F. Prog Surf Sci. 2000; 65:151.
11. Zhang J, Li Y, Zhang X, Yang B. Adv Mater. 2010; 22:4249. [PubMed: 20803529]
12. Mulkens J, Flagello D, Streefkerk B, Graeupner P. J MicroNanolithography MEMS MOEMS. 2004; 3:104.
13. Terris BD, Mamin HJ, Rugar D, Studenmund WR, Kino GS. Appl Phys Lett. 1994; 65:388.
14. Ghislain LP, Elings VB, Crozier KB, Manalis SR, Minne SC, Wilder K, Kino GS, Quate CF. Appl Phys Lett. 1999; 74:501.
15. Lewis A, Isaacson M, Harootunian A, Muray A. Ultramicroscopy. 1984; 13:227.
16. Pohl DW, Denk W, Lanz M. Appl Phys Lett. 1984; 44:651.
17. Ozcan A, Cubukcu E, Bilenca A, Crozier KB, Bouma BE, Capasso F, Tearney GJ. Nano Lett. 2006; 6:2609. [PubMed: 17090100]
18. Ozcan A, Cubukcu E, Bilenca A, Bouma BE, Capasso F, Tearney GJ. IEEE J Sel Top Quantum Electron. 2007; 13:1721.
19. Neumann A, Kuznetsova Y, Brueck SRJ. Opt Express. 2008; 16:20477. [PubMed: 19065186]
20. Kuznetsova Y, Neumann A, Brueck SR. Opt Express. 2007; 15:6651. [PubMed: 19546975]
21. Granero L, Micó V, Zalevsky Z, García J. Opt Express. 2009; 17:15008. [PubMed: 19687979]
22. Paturzo M, Merola F, Grilli S, De Nicola S, Finizio A, Ferraro P. Opt Express. 2008; 16:17107. [PubMed: 18852822]
23. Paturzo M, Ferraro P. Opt Lett. 2009; 34:3650. [PubMed: 19953150]
24. Jacob Z, Alekseyev LV, Narimanov E. Opt Express. 2006; 14:8247. [PubMed: 19529199]
25. Liu Z, Lee H, Xiong Y, Sun C, Zhang X. Science. 2007; 315:1686. [PubMed: 17379801]
26. Poddubny A, Iorsh I, Belov P, Kivshar Y. Nat Photonics. 2013; 7:948.
27. Fang N, Lee H, Sun C, Zhang X. Science. 2005; 308:534. [PubMed: 15845849]
28. Hell S, Wichmann J. Opt Lett. 1994; 19:780. [PubMed: 19844443]

29. Betzig E, Patterson GH, Sougrat R, Lindwasser OW, Olenych S, Bonifacino JS, Davidson MW, Lippincott-Schwartz J, Hess HF. Science. 2006; 313:1642. [PubMed: 16902090]
30. Rust MJ, Bates M, Zhuang X. Nat Methods. 2006; 3:793. [PubMed: 16896339]
31. Adamczyk Z, Nattich-Rak M, Sadowska M, Michna A, Szczepaniak K. Colloids Surf Physicochem Eng Asp. 2013; 439:3.
32. Muangnapoh T, Weldon AL, Gilchrist JF. Appl Phys Lett. 2013; 103:181603.
33. Grzelczak M, Vermant J, Furst EM, Liz-Marzán LM. ACS Nano. 2010; 4:3591. [PubMed: 20568710]
34. Venables JA, Spiller GDT, Hanbucken M. Rep Prog Phys. 1984; 47:399.
35. Solomon GS, Trezza JA, Marshall AFJ, Harris JS. Phys Rev Lett. 1996; 76:952. [PubMed: 10061593]
36. Mirkin CA, Letsinger RL, Mucic RC, Storhoff JJ. Nature. 1996; 382:607. [PubMed: 8757129]
37. Ke Y, Ong LL, Shih WM, Yin P. Science. 2012; 338:1177. [PubMed: 23197527]
38. Qi H, Ghodousi M, Du Y, Grun C, Bae H, Yin P, Khademhosseini A. Nat Commun. 2013; 4
39. Du Y, Lo E, Ali S, Khademhosseini A. Proc Natl Acad Sci. 2008; 105:9522. [PubMed: 18599452]
40. Shenton W, Davis SA, Mann S. Adv Mater. 1999; 11:449.
41. Ulman A. Chem Rev. 1996; 96:1533. [PubMed: 11848802]
42. Syms RRA, Yeatman EM, Bright VM, Whitesides GM. J Microelectromechanical Syst. 2003; 12:387.
43. Brinker CJ, Lu Y, Sellinger A, Fan H. Adv Mater. 1999; 11:579.
44. Kumnorkaew P, Ee Y-K, Tansu N, Gilchrist JF. Langmuir. 2008; 24:12150. [PubMed: 18533633]
45. Huo Y, Fesenmaier CC, Catrysse PB. Opt Express. 2010; 18:5861. [PubMed: 20389603]
46. Artzner GE. Opt Eng. 1992; 31:1311.
47. Levoy M, Zhang Z, Mcdowall I. J Microsc. 2009; 235:144. [PubMed: 19659909]
48. Ng R, Levoy M, Brédif M, Duval G, Horowitz M, Hanrahan P. Light Field Photography with a Hand-Held Plenoptic Camera. 2005
49. Cho M, Daneshpanah M, Moon I, Javidi B. Proc IEEE. 2011; 99:556.
50. Lee LP, Szema R. Science. 2005; 310:1148. [PubMed: 16293752]
51. Aizenberg J, Tkachenko A, Weiner S, Addadi L, Hendler G. Nature. 2001; 412:819. [PubMed: 11518966]
52. Huang J-Y, Lu Y-S, Yeh JA. Opt Express. 2006; 14:10779. [PubMed: 19529487]
53. Brody JP, Quake SR. Appl Phys Lett. 1999; 74:144.
54. Schwartz JJ, Stavrakis S, Quake SR. Nat Nanotechnol. 2010; 5:127. [PubMed: 20023643]
55. Mudanyali O, Bishara W, Ozcan A. Opt Express. 2011; 19:17378. [PubMed: 21935102]
56. Bishara W, Sikora U, Mudanyali O, Ting-Wei S, Yaglidere O, Luckhart S, Ozcan A. Lab Chip. 2011; 11:1276. [PubMed: 21365087]
57. Greenbaum A, Luo W, Su T-W, Göröcs Z, Xue L, Isikman SO, Coskun AF, Mudanyali O, Ozcan A. Nat Methods. 2012; 9:889. [PubMed: 22936170]
58. Su T-W, Xue L, Ozcan A. Proc Natl Acad Sci. 2012; 109:16018. [PubMed: 22988076]
59. Isikman SO, Bishara W, Zhu H, Ozcan A. Appl Phys Lett. 2011; 98:161109. [PubMed: 21580801]
60. Mudanyali O, McLeod E, Luo W, Greenbaum A, Coskun AF, Hennequin Y, Allier CP, Ozcan A. Nat Photonics. 2013; 7:247.
61. McLeod E, Luo W, Mudanyali O, Greenbaum A, Ozcan A. Lab Chip. 2013; 13:2028. [PubMed: 23592185]
62. Allier CP, Hiernard G, Poher V, Dinten JM. Biomed Opt Express. 2010; 1:762. [PubMed: 21258507]
63. Hennequin Y, Allier CP, McLeod E, Mudanyali O, Migliozzi D, Ozcan A, Dinten J-M. ACS Nano. 2013; 7:7601. [PubMed: 23889001]
64. Mason DR, Jouravlev MV, Kim KS. Opt Lett. 2010; 35:2007. [PubMed: 20548368]
65. Kim M-S, Scharf T, Haq MT, Nakagawa W, Herzig HP. Opt Lett. 2011; 36:3930. [PubMed: 21964145]

66. Kim M-S, Scharf T, Nguyen D, Keeler E, Rydberg S, Nakagawa W, Osowiecki G, Voelkel R, Herzig HP. J MicroNanolithography MEMS MOEMS. 2013; 12:023015.
67. Guo H, Han Y, Weng X, Zhao Y, Sui G, Wang Y, Zhuang S. Opt Express. 2013; 21:2434. [PubMed: 23389224]
68. Wang Z, Guo W, Li L, Luk'yanchuk B, Khan A, Liu Z, Chen Z, Hong M. Nat Commun. 2011; 2:218. [PubMed: 21364557]
69. Mcleod E, Arnold CB. Nat Nanotechnol. 2008; 3:413. [PubMed: 18654565]
70. McLeod E, Arnold CB. Opt Express. 2009; 17:3640. [PubMed: 19259204]
71. Jang J-W, Zheng Z, Lee O-S, Shim W, Zheng G, Schatz GC, Mirkin CA. Nano Lett. 2010; 10:4399. [PubMed: 20879780]
72. Fletcher DA, Goodson KE, Kino GS. Opt Lett. 2001; 26:399. [PubMed: 18040333]
73. Min SK, Cho Y, Mason DR, Lee JY, Kim KS. J Phys Chem C. 2011; 115:16247.
74. Duan Y, Barbastathis G, Zhang B. Opt Lett. 2013; 38:2988. [PubMed: 24104628]
75. Lee JY, Hong BH, Kim WY, Min SK, Kim Y, Jouravlev MV, Bose R, Kim KS, Hwang I-C, Kaufman LJ, Wong CW, Kim P, Kim KS. Nature. 2009; 460:498.
76. Lee S-K, Lee K-C, Lee SS. J Micromechanics Microengineering. 2002; 12:334.
77. Vlad A, Huynen I, Melinte S. Nanotechnology. 2012; 23:285708. [PubMed: 22728662]
78. Piner RD, Zhu J, Xu F, Hong S, Mirkin CA. Science. 1999; 283:661. [PubMed: 9924019]
79. Zhang X, Ren J, Yang H, He Y, Tan J, Qiao GG. Soft Matter. 2012; 8:4314.
80. Ren H, Xu S, Liu Y, Wu S-T. J Mater Chem C. 2013; 1:7453.
81. Kang D, Pang C, Kim SM, Cho HS, Um HS, Choi YW, Suh KY. Adv Mater. 2012; 24:1709. [PubMed: 22388770]
82. Smolyaninova VN, Smolyaninov II, Kildishev AV, Shalaev VM. Opt Lett. 2010; 35:3396. [PubMed: 20967078]
83. Smolyaninov II, Elliott J, Zayats AV, Davis CC. Phys Rev Lett. 2005; 94:057401. [PubMed: 15783692]
84. Leonhardt U. New J Phys. 2009; 11:093040.
85. Verma A, Sharma A. Adv Mater. 2010; 22:5306. [PubMed: 20872412]
86. Verma A, Sharma A. Soft Matter. 2011; 7:11119.
87. Verma A, Sharma A. Curr Sci. 2013; 00113891–104:1037.
88. Dietzel M, Troian SM. Phys Rev Lett. 2009; 103:074501. [PubMed: 19792647]
89. McLeod E, Liu Y, Troian SM. Phys Rev Lett. 2011; 106:175501. [PubMed: 21635044]
90. Rajasekharan R, Wilkinson TD, Hands PJW, Dai Q. Nano Lett. 2011; 11:2770. [PubMed: 21657239]
91. Dai Q, Rajasekharan R, Butt H, Qiu X, Amaragtunga G, Wilkinson TD. Small. 2012; 8:2501. [PubMed: 22696434]
92. Beller DA, Gharbi MA, Honglawan A, Stebe KJ, Yang S, Kamien RD. Phys Rev X. 2013; 3:041026.
93. Jeon S, Jang JY, Youn JR, Jeong J, Brenner H, Song YS. Sci Rep. 2013; 3
94. Khokhra R, Kumar M, Rawat N, Barman PB, Jang H, Kumar R, Lee H-N. J Opt. 2013; 15:125714.
95. Vellekoop IM, Mosk AP. Opt Lett. 2007; 32:2309. [PubMed: 17700768]
96. Popoff SM, Lerosey G, Carminati R, Fink M, Boccara AC, Gigan S. Phys Rev Lett. 2010; 104:100601. [PubMed: 20366410]
97. Zhang Q, Li KH, Choi HW. Appl Phys Lett. 2012; 100:061120.
98. Ee Y-K, Kumnorkaew P, Arif RA, Tong H, Zhao H, Gilchrist JF, Tansu N. IEEE J Sel Top Quantum Electron. 2009; 15:1218.
99. Sun B, Zhao L, Wei T, Yi X, Liu Z, Wang G, Li J, Yi F. Opt Express. 2012; 20:18537. [PubMed: 23038492]
100. Son T, Jung K-Y, Park J. Curr Appl Phys. 2013; 13:1042.
101. Lu Z, Yin Y. Chem Soc Rev. 2012; 41:6874. [PubMed: 22868949]
102. Kim J, Piao Y, Hyeon T. Chem Soc Rev. 2009; 38:372. [PubMed: 19169455]

103. Sarti S, Bordi F. Mater Lett. 2013; 109:134.
104. Lesnyak V, Gaponik N, Eychmüller A. Chem Soc Rev. 2013; 42:2905. [PubMed: 23165911]
105. Kuno M, Fromm DP, Hamann HF, Gallagher A, Nesbitt DJ. J Chem Phys. 2001; 115:1028.
106. Frantsuzov P, Kuno M, Jankó B, Marcus RA. Nat Phys. 2008; 4:519.
107. Wei Q, McLeod E, Qi H, Wan Z, Sun R, Ozcan A. Sci Rep. 2013; 3:1699. [PubMed: 23608952]
108. Barrow SJ, Funston AM, Wei X, Mulvaney P. Nano Today. 2013; 8:138.
109. Wei Q, Nagi R, Sadeghi K, Feng S, Yan E, Ki SJ, Caire R, Tseng D, Ozcan A. ACS Nano. 2014
110. Ando J, Yano T, Fujita K, Kawata S. Phys Chem Chem Phys. 2013; 15:13713. [PubMed: 23861007]

Biographies

Euan McLeod: earned his B.S. from the California Institute of Technology and his Ph.D. from Princeton University. At Princeton, he worked with Professor Craig Arnold in nanoscale laser materials processing. He is currently a Postdoctoral Scholar at UCLA, working in the Bio- and Nano-Photonics laboratory under Professor Aydogan Ozcan. His research interests lie at the intersection of soft-materials and nano-photonics.

Aydogan Ozcan: is the Chancellor's Professor at UCLA leading the Bio- and Nano-Photonics Laboratory at the Electrical Engineering and Bioengineering Departments. Dr. Ozcan holds 22 issued patents (all of which are licensed) and >15 pending patent applications and is also the author of one book and the co-author of more than 350 peer reviewed research articles in major scientific journals and conferences. Dr. Ozcan is a Fellow of SPIE and OSA, and has received major awards including the Presidential Early Career Award for Scientists and Engineers (PECASE), SPIE Biophotonics Technology Innovator Award, SPIE Early Career Achievement Award, ARO Young Investigator Award, NSF CAREER Award, NIH Director's New Innovator Award, ONR Young Investigator Award, IEEE Photonics Society Young Investigator Award and MIT's TR35 Award for his seminal contributions to near-field and on-chip imaging, and telemedicine based diagnostics. Dr. Ozcan is also the recipient of the National Geographic Emerging Explorer Award,

National Academy of Engineering (NAE) The Grainger Foundation Frontiers of Engineering Award, Popular Science Brilliant 10 Award, Gates Foundation Grand Challenges Award, Popular Mechanics Breakthrough Award, Netexplorateur Award, Microscopy Today Innovation Award, and the Wireless Innovation Award organized by the Vodafone Americas Foundation as well as the Okawa Foundation Award.

HIGHLIGHTS

- Nano-imaging enabled by self-assembly provides strong signal-to-noise and resolution below ~200nm.
- Self-assembly harnesses random motion for fabrication.
- Self-assembly has been used to fabricate nano-imaging lenses and other nano-structures.

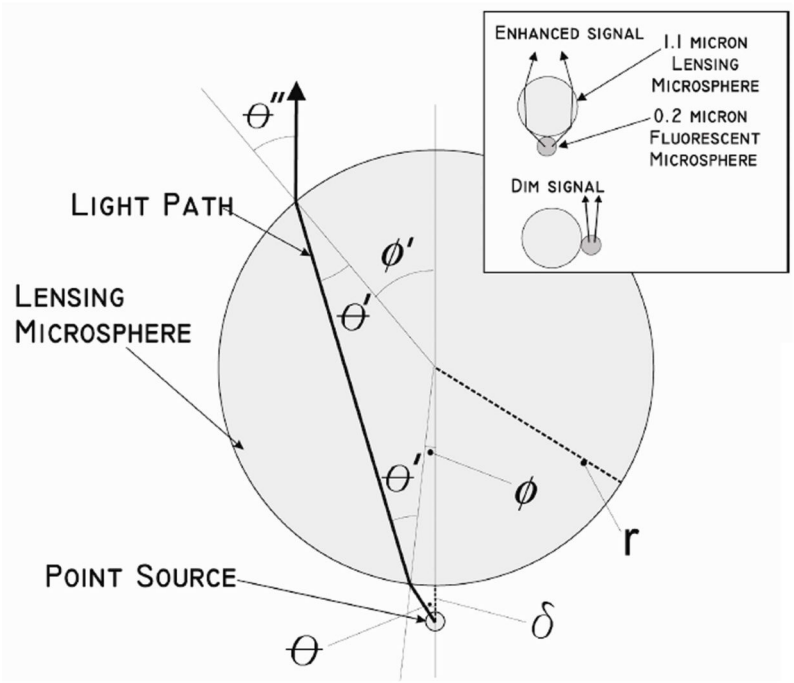

Figure 1. Self-assembled rotational probe

In this probe, a large micro-lens is used to enhance the captured fluorescence signal from a single nanoparticle. When suspended in a fluid, the probe will freely rotate and the observed signal will fluctuate depending on the orientation of the probe, providing a mechanism to measure probe rotation rate in different fluids. Image reproduced with permission from [53].

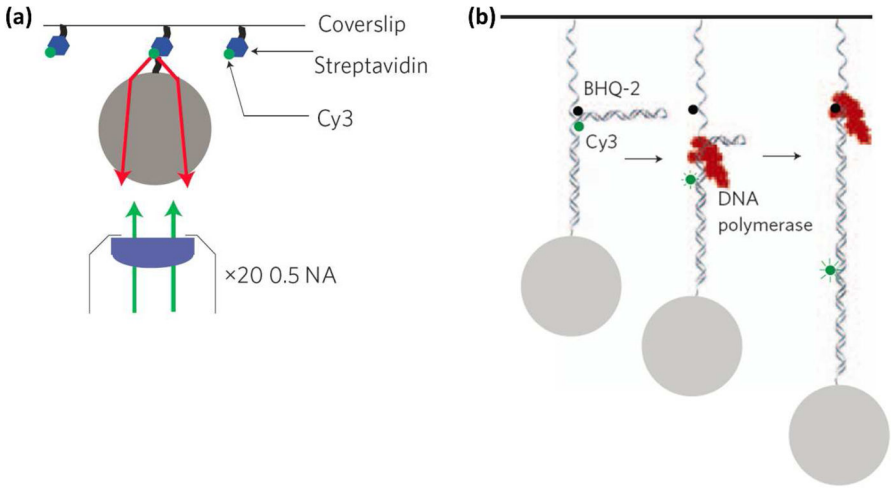

Figure 2. Microspheres used to enhance the signal from single fluorescent molecules

Individual Cy3 molecules coupled to streptavidin (a) or DNA (b) molecules are detected in a fluorescent microscope. Typically these nano-scale individual fluorescent molecules would not produce a strong enough emission to be imaged by low-NA wide-field microscope objectives. However, the incorporation of microspheres as signal enhancers makes this possible. Image reproduced with permission from [54].

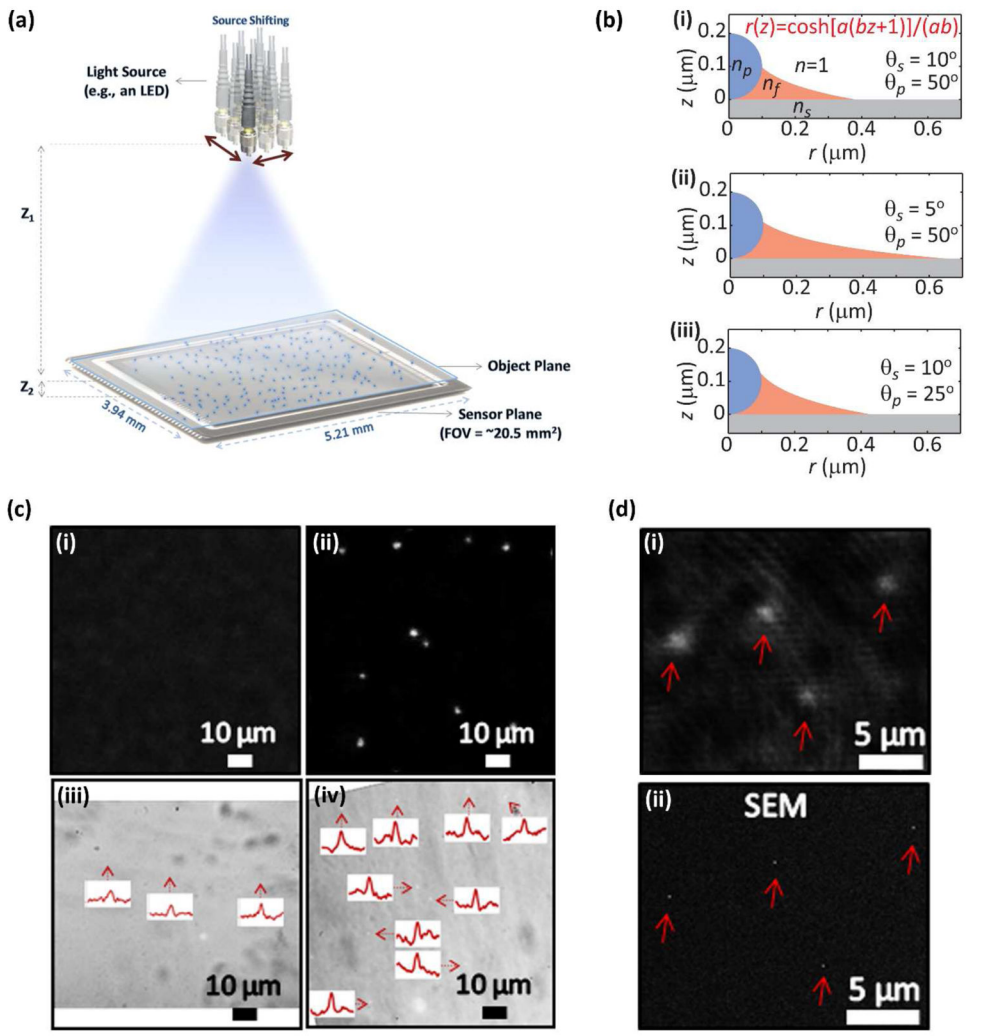

Figure 3. Self-assembled catenoid nano-lenses for nano-particle and virus imaging in lensfree holographic microscopy

(a) Typical lensfree holographic setup where a partially-coherent light source generates an in-line holographic image of the sample directly on the image sensor without the use of lenses. (b) Minimal surface catenoid lens shapes of the self-assembled nano-lenses formed around spherical particles. (c) Experimental verification that self-assembled nano-lenses enable otherwise undetectable 95 nm particles to be imaged. (i) and (ii) show the holographic reconstructions of 95 nm particles without, and with, nano-lenses, respectively. (iii) and (iv) show optical microscope comparisons that confirm the presence of particles in the samples. (d) Single adeno viruses imaged using self-assembled nano-lenses (i), with SEM verification of particle locations and sizes (ii). Image reproduced with permission from [60].

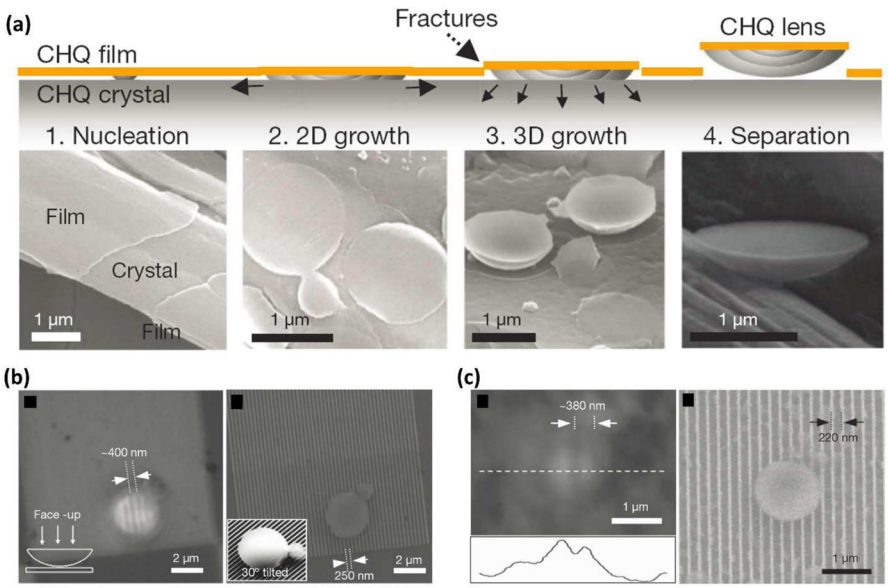

Figure 4. Self-assembled nano-lenses grown from CHQ molecules

Plano-convex nano-lenses are fabricated and used to image features below the diffraction limit. (a) Illustrates the fabrication procedure. (b) shows the resolution of 250 nm pitch lines. At the right is an SEM image of the same structure. (c) shows the resolution of 220 nm pitch (period) lines, with an SEM comparison. Reproduced with permission from [75].

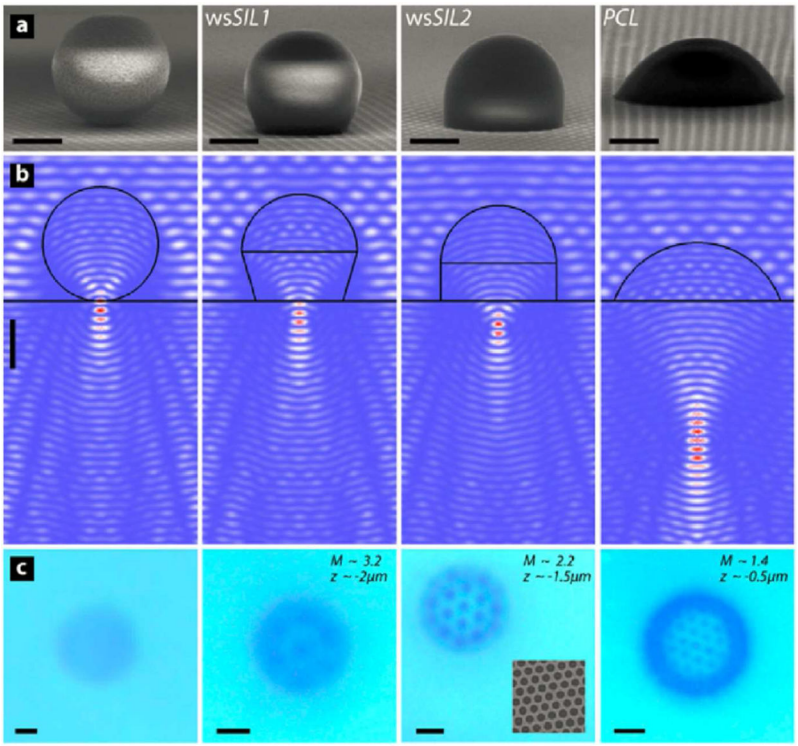

Figure 5. Various lens shapes self-assembled via thermal reflow and used for nano-imaging

(a) shows oblique SEM images of the lenses. (b) Simulated results for focused light intensity distribution. (c) Experimental results for the imaging of 180 nm holes placed at a pitch of 330 nm. Scale bars 1 μm. Image reproduced with permission from [77].

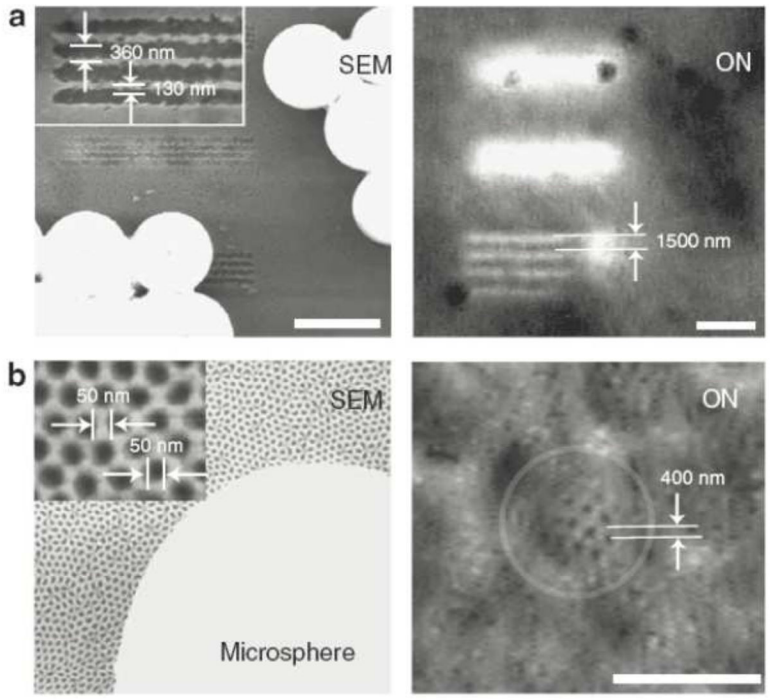

Figure 6. Self-assembled microspheres used as superlenses

In (a), 490 nm pitch lines are resolved in the regions below the microspheres. The SEM comparison is shown on the left, and the optical image on the right. In (b), microspheres enable the resolution of 50-nm half-pitch structures. Image reproduced with permission from [68].

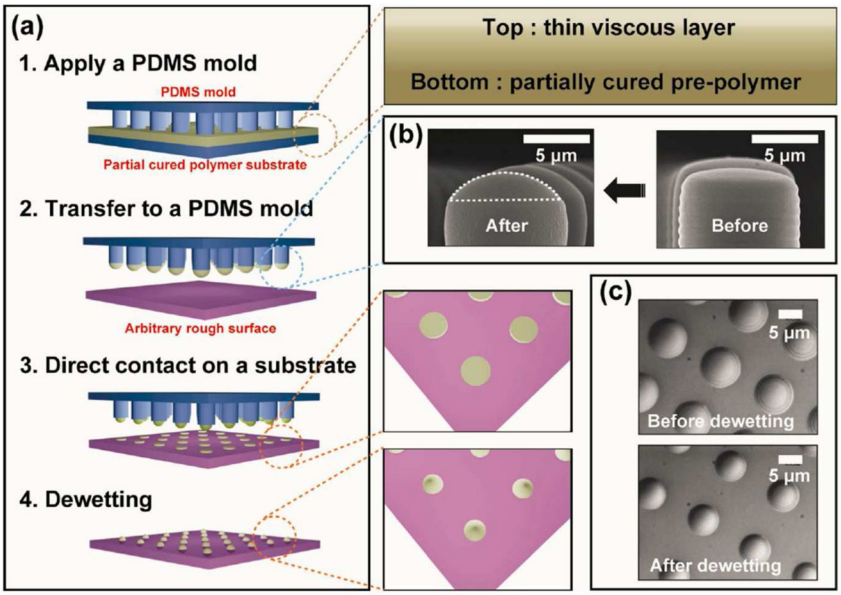

Figure 7. Nano-lens material transfer using a PDMS stamp followed by lens-shape self-assembly

In this study, surface treatments were used to form a variety of lens shapes with different contact angles, which manifested after dewetting. The overall procedure is depicted in (a), with zoom-ins of individual steps in (b) and (c). These lenses were used to resolve features with half-pitches as small as 250 nm. Image reproduced with permission from [81].

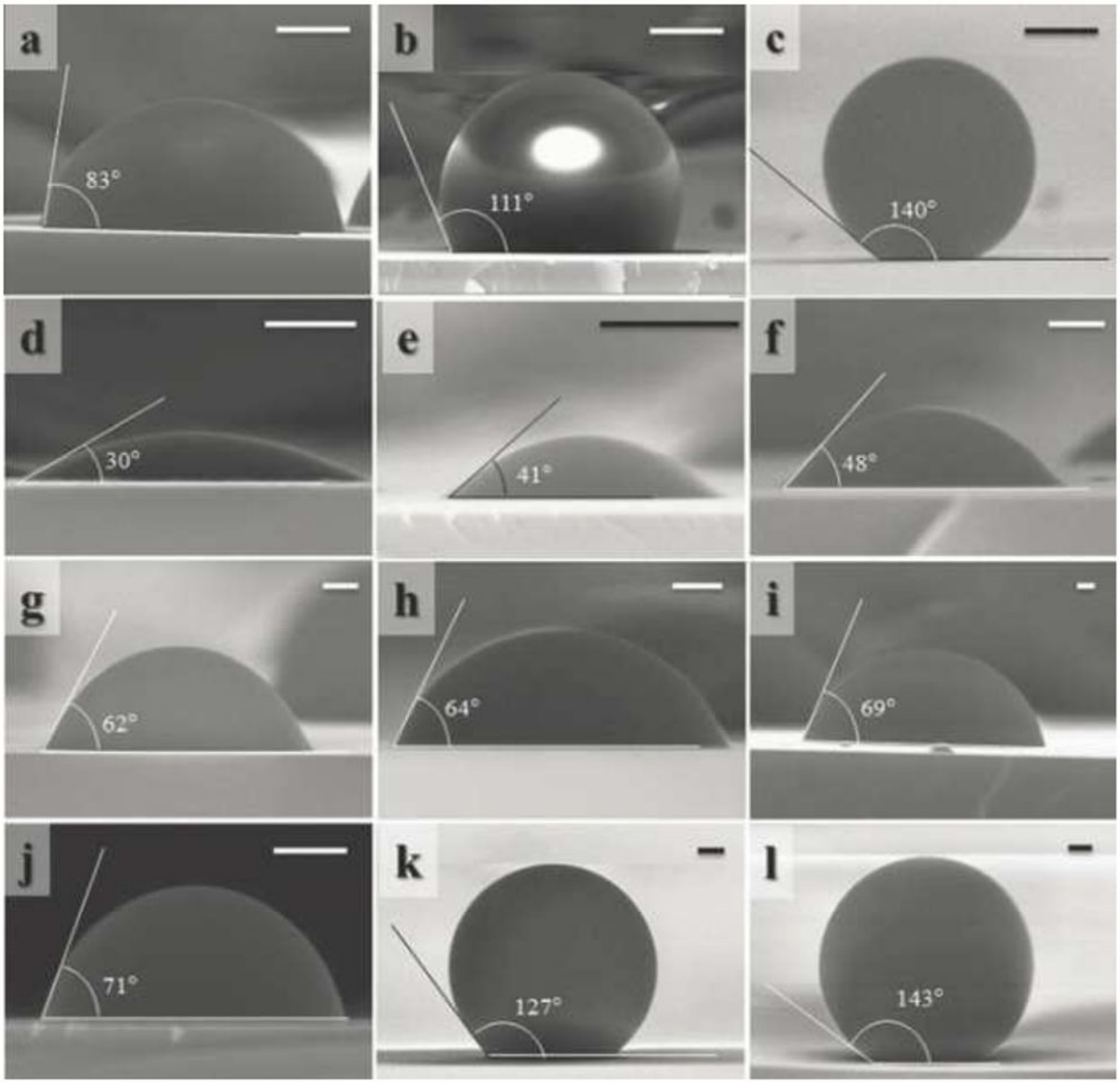

Figure 8. Various nano-lens shapes fabricated using dewetting

Here, a method of fabricating lenses of different shapes and sizes is illustrated. In all subfigures, the lens material is polystyrene and the substrate is silicon. However, different initial film thicknesses, temperatures, and annealing times lead to different lens shapes. These types of lenses may be suited to various applications requiring different resolutions and fields of view. Scale bar is 200 nm. Image reproduced with permission from [85].

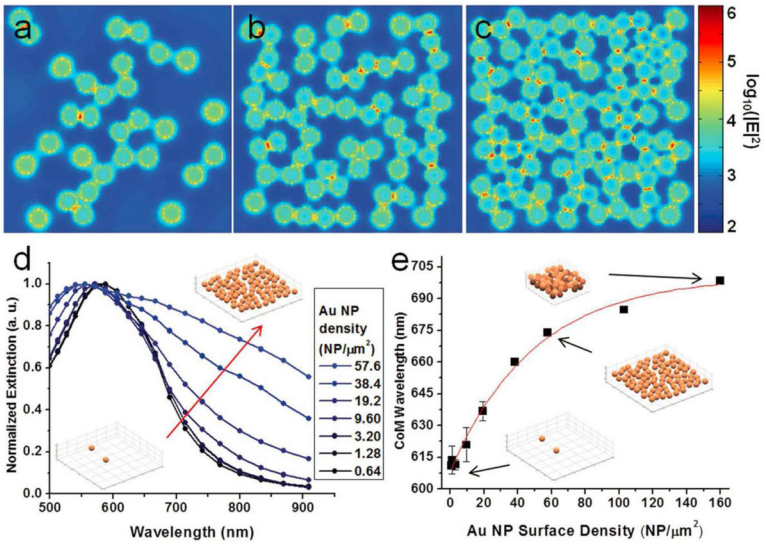

Figure 9. Clustering-induced changes in nano-particle plasmonic resonance

(a–c) show the gold nanoparticle configurations simulated using FDTD methods, along with the field levels found between the particles. (d) and (e) quantify the results of these simulations, which show that the extinction spectra of theses assemblies shifts toward the red at higher cluster densities. (e) shows the shift in the center-of-mass (CoM) wavelength of the extinction spectra. This shift can be used to identify nanoscopic domains in biological or chemical samples with higher densities of nanoparticles. Image reproduced with permission from [107].